# Boundary Forces in lattice Boltzmann: Analysis of Momentum Exchange algorithm

Alfonso Caiazzo [a] Michael Junk [b]

[a] *Fraunhofer ITWM, Fraunhofer-Platz 1 D-67663, Kaiserslautern, Germany*

[b] *FB Mathematik und Statistik Universität Konstanz, Postfach D194, D-78457 Konstanz, Germany*

**Abstract**

When lattice Boltzmann methods are used to simulate fluid-structure interaction problems, they need to be coupled with additional routines to evaluate the boundary forces without destroying the efficiency and accuracy of the original method. We use the asymptotic expansion technique to analyze one such approach, the *Momentum Exchange algorithm*, investigating in detail its properties, whether it can be improved and in which cases it can be successfully used. A statement regarding the accuracy is presented, together with results of numerical tests which illustrate the theoretical considerations.

*Key words:* lattice Boltzmann equation; fluid-boundary interaction, momentum exchange algorithm.

## 1 Introduction

In recent years, applications of the lattice Boltzmann method (LBM) have been extending towards fluid-structure interaction problems, taking advantage of the ability of the LBM in modeling flows through complex geometries. Such problems, however, require special routines to evaluate the *boundary forces* due to the fluid flow.

Since the best characteristics of the LBM lie in its *efficiency*, the additional algorithm should be able to preserve this property, in order to keep the LBM numerically competitive. We focus on the *Momentum Exchange algorithm* (pro-

*Email addresses:* caiazzo@itwm.fhg.de (Alfonso Caiazzo), Michael.Junk@uni-konstanz.de (Michael Junk).

posed in [1]), which models the fluid-boundary interaction based on simple particle dynamics, and which requires only a low additional computational effort. In fact, this method has been used in numerical simulations [2,3] but, to the knowledge of the authors, has not been investigated theoretically in depth. In this paper, we present an *asymptotic analysis* of the algorithm, discussing in general the *consistency* and the *accuracy* of the method.

In section 2 we set up the flow model and the benchmarks. LBM and MEA are described in section 3. Section 4 contains a first analysis of the MEA, together with the numerical tests. Finally, in section 4.1 we analyze in detail the evaluation of local forces and enunciate a theoretical result regarding the accuracy of the MEA.

## 2 The flow model

In order to study the boundary force evaluation within the lattice Boltzmann method, we consider a two-dimensional flow in the unit square $\Omega = [0,1)^2$ with periodic boundary conditions. A disk $\Omega_S(t) \subset \Omega$ with radius $R < 1$ is considered as a solid body which is separated from the fluid region $\Omega_F(t)$ by the common interface $\Gamma(t)$, i.e. $\Omega = \Omega_F \cup \Gamma \cup \Omega_S$ (see fig. 1a). Physically, this situation models a cross section through a flow around a periodic array of long cylinders. For this reason, we refer to the problem as *cylinder-in-flow* (CiF).

For simplicity, we assume that $\Omega_S(t)$ moves with a given velocity along a prescribed path. This will help us to formulate simple test problems for which the exact boundary forces are known. If the state of the system is known at the initial time $t = 0$, the dynamics of the fluid can be described by an incompressible Navier-Stokes problem with initial and boundary values

$$\begin{aligned} &\begin{cases} \nabla \cdot \mathbf{u} = 0 \\ \partial_t \mathbf{u} + \nabla p + \nabla \cdot (\mathbf{u} \otimes \mathbf{u}) = \nu \nabla^2 \mathbf{u} + \mathbf{G} \end{cases} && t > 0,\ \mathbf{x} \in \Omega_F(t) \\ &\mathbf{u}(t, \mathbf{x}) = \mathbf{u}_B(t, \mathbf{x}), \quad t > 0,\ \mathbf{x} \in \Gamma(t) \\ &\mathbf{u}(0, \mathbf{x}) = \mathbf{u}_0(\mathbf{x}) \quad \mathbf{x} \in \Omega_F(0) \end{aligned} \tag{1}$$

where $\mathbf{u}_B(t, \mathbf{x})$ is the given velocity of the interface point $\mathbf{x} \in \Gamma(t)$ at time $t$ and $\mathbf{G}$ is the volume force acting on the fluid [1].

[1] We consider incompressible flows where the density of the fluid is given by a constant reference density $\rho_0$. In the formulation of the Navier-Stokes equation (1) we denote with $p$ the *kinematic* pressure, which is defined as the *dynamic* pressure divided by the density. Using a scaling where $\rho_0 = 1$, the two quantities coincide.

The *total boundary force*[2] is evaluated according to

$$\mathbf{F}_S(t) = \int_{\Gamma(t)} (-p(t,\mathbf{x})\mathbf{I} + \mathbf{S}(t,\mathbf{x})) \cdot \mathbf{n}(\mathbf{x}) d\sigma(\mathbf{x}) \tag{2}$$

where

$$\mathbf{S} = \nu \left( \nabla \mathbf{u} + \nabla \mathbf{u}^T \right) \tag{3}$$

is the viscous stress tensor and $\mathbf{n}$ the normal vector to $\Gamma$ pointing out of the solid domain. If $\mathbf{t}$ denotes the tangential vector to $\Gamma$, which is obtained by following the interface counterclockwise, the *local stresses* are

$$f_{\mathbf{t}} = (\mathbf{S} \cdot \mathbf{n}) \cdot \mathbf{t}, \quad f_{\mathbf{n}} = -p + (\mathbf{S} \cdot \mathbf{n}) \cdot \mathbf{n}. \tag{4}$$

In order to test the lattice Boltzmann algorithm presented below, we use two simple exact solutions of (1) denoted $\mathrm{CiF}_0$ and $\mathrm{CiF}_1$. In the case of $\mathrm{CiF}_0$, we move the disk with constant velocity $\mathbf{u}_0$ in a flow with the same constant velocity, zero pressure, and vanishing body force $\mathbf{G} = 0$. As a consequence, the local stresses vanish and the total boundary force is zero.

In the case $\mathrm{CiF}_1$, we again move the body with a constant velocity $\mathbf{u}_0$ in the constant flow field $\mathbf{u}(t,\mathbf{x}) = \mathbf{u}_0$. However, to obtain a non-trivial local force, we choose a periodic function $p_0$ and define the body force $\mathbf{G} = \nabla p_0$ which generates a pressure $p(t,\mathbf{x}) = p_0(\mathbf{x})$. For the particular choice

$$p_0(x,y) = \sin(2\pi x)\cos(2\pi y) \tag{5}$$

we obtain

$$\begin{aligned} &f_{\mathbf{t}}(t,\theta) = 0, \\ &f_{\mathbf{n}}(t,\theta) = -\sin(2\pi(x_C(t) + R\cos\theta))\cos(2\pi(y_C(t) + R\sin\theta)). \end{aligned} \tag{6}$$

## 3 The lattice Boltzmann method

The lattice Boltzmann method can be viewed as a discretized form of a finite velocity model Boltzmann equation

$$\partial_t f_i + \mathbf{c}_i \cdot \nabla f_i = J_i(f), \quad i = 0, \ldots, N \tag{7}$$

[2] The total torque acting on the solid,

$$\mathbf{T}(t) = \int_{\Gamma(t)} (\mathbf{x} - \mathbf{x}_{CM}) \times [(-p(t,\mathbf{x})\mathbf{I} + \mathbf{S}(t,\mathbf{x})) \cdot \mathbf{n}(\mathbf{x})] \; d\sigma(\mathbf{x}),$$

could be considered in the same way.

where $\mathbb{V} = \{\mathbf{c}_i\}_{i=0,\dots,N}$ is the finite velocity set. In equation (7), the variable $f_i(t, \mathbf{x})$ represents the mass density distribution of the particles moving in direction $\mathbf{c}_i$, at time $t$ and position $\mathbf{x}$. On the right hand side, the *collision* operator $J_i(f)$ models the effects of the collisions between particles, producing variations in the distributions. In the presented numerical results, the two-dimensional $D2Q9$ model has been used with velocities

$$\begin{aligned} &\mathbf{c}_0 = (0,0), \\ &\mathbf{c}_1 = (1,0), \quad \mathbf{c}_2 = (1,1), \quad \mathbf{c}_3 = (0,1), \quad \mathbf{c}_4 = (-1,1), \\ &\mathbf{c}_5 = (-1,0), \quad \mathbf{c}_6 = (-1,-1), \quad \mathbf{c}_7 = (0,-1), \quad \mathbf{c}_8 = (1,-1). \end{aligned} \tag{8}$$

Details and overviews of the lattice Boltzmann method, as well as description of this model, can be found in [4].

In describing the LBM a *dimensionless lattice units reference system* is used, where space and time units are represented by grid size and time step. In problem relevant scales, time step $\Delta t$ and space step $h$ are related by the *diffusive scaling* $\Delta t = h^2$ which is a prerequisite to recover the incompressible Navier-Stokes equations in the limit (see [5] for a detailed discussion). The numerical results of LBM, at time $t_n = nh^2$ and at position $\mathbf{x}_\mathbf{j} = h\mathbf{j}$, are expressed by functions $\hat{f}_i(n, \mathbf{j}) : \mathbb{N} \times \mathbb{Z}^2 \to \mathbb{R}$. With the $BGK$ approximation of $J_i$ on the right hand side of (7), the general iteration of the algorithm reads

$$\hat{f}_i(n+1, \mathbf{j} + \mathbf{c}_i) = \hat{f}_i(n, \mathbf{j}) + \frac{1}{\tau}(f_i^{eq}(\hat{f}) - \hat{f}_i)(n, \mathbf{j}) + g_i(n, \mathbf{j}). \tag{9}$$

The *equilibrium distribution* $f^{eq}$ is a function of $\hat{f}$, through the moments $\hat{\rho} = \sum_i \hat{f}_i$ and $\hat{\mathbf{u}} = \sum_i \mathbf{c}_i \hat{f}_i$, denoted as

$$f_i^{eq}(f) = H_i^{eq}\left(\rho(f), \mathbf{u}(f)\right). \tag{10}$$

The expression of $H^{eq}$ depends on the model. For the considered $D2Q9$ model (as well as for the three-dimensional $D3Q15$), it reads

$$H_i^{eq}(\rho, \mathbf{u}) = f_i^* \left( \rho + c_s^{-2} \mathbf{c}_i \cdot \mathbf{u} + \frac{c_s^{-4}}{2} \left( |\mathbf{c}_i \cdot \mathbf{u}|^2 - c_s^2 \mathbf{u}^2 \right) \right). \tag{11}$$

The relaxation time $\tau$ in equation (9) is related to a dimensionless viscosity through $\nu = c_s^2(\tau - \frac{1}{2})$. Model depending are the lattice sound speed $c_s$ and the weights $f_i^*$ (see [4]). The term $g_i$ is responsible for the force

$$g_i(n, \mathbf{j}) = c_s^{-2} h^3 f_i^* \mathbf{c}_i \cdot \mathbf{G}(t_n, \mathbf{x}_\mathbf{j}).$$

In practice, the algorithm is implemented by splitting collision and transport,

introducing the *post-collisional* distribution

$$\hat{f}_i^c(n,\mathbf{j}) = \hat{f}_i(n,\mathbf{j}) + \frac{1}{\tau}(f_i^{eq}(\hat{f}) - \hat{f}_i)(n,\mathbf{j}) + g_i(n,\mathbf{j}), \tag{12}$$

corresponding to the right hand side of equation (9).

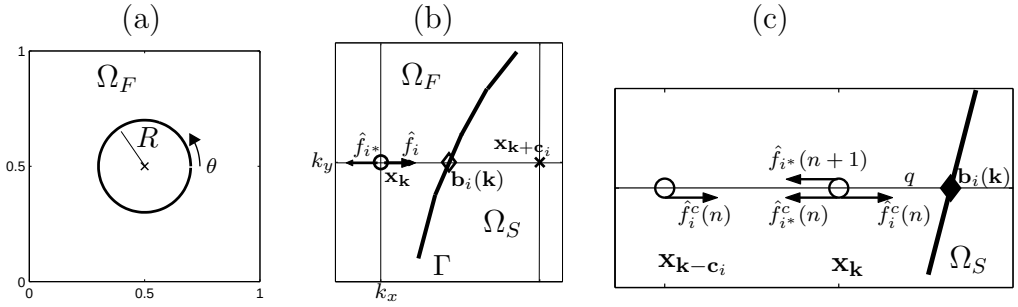


Figure 1. **(a)** The CiF problem. In a periodic square $[0,1]\times[0,1]$ a circle of radius $R=0.2$, located in the center, interacts with the flow. The coordinate on the interface is denoted with $\theta$. **(b)** A grid point $\mathbf{x_k}\in\Omega_F$ ($\circ$) is called *boundary node* if it has at least one neighbor $\mathbf{x_k}+h\mathbf{c}_i$ ($\times$) in the solid domain $\Omega_S$. The *outgoing* direction $i$ will then *intersect* the boundary $\Gamma$ at the point $\mathbf{b}_i(\mathbf{k})$ ($\diamond$). **(c)** To update $\hat{f}_{i^*}$ according to the Dirichlet condition, the $BFL$ rule uses a combination of the populations *after collision* at two neighbor nodes, involving the distance $q$ between the boundary and $\mathbf{x_k}$, and the velocity at the point $\mathbf{b}_i(\mathbf{k})$ on the boundary.

**Boundary conditions.** To include the Dirichlet boundary conditions for the average velocity, an additional boundary algorithm has to be coupled to (9). Among the available approaches, we consider the $BFL$ rule, described in [6]. From the computational point of view, we consider those grid points as *fluid nodes* which belong to the fluid domain $\Omega_F$ or to the interface $\Gamma$. According to the notation in figure 1b-c, for a *boundary node* $\mathbf{x_k}=h\mathbf{k}\in\Omega_F\cup\Gamma$ such that $\mathbf{x_k}+h\mathbf{c}_i\in\Omega_S$, we define

$$\hat{f}_{i^*}(n+1,\mathbf{k}) = \begin{cases} 2q\hat{f}_i^c(n,\mathbf{k}) + (1-2q)\hat{f}_i^c(n,\mathbf{k}-\mathbf{c}_i) + \\ \qquad 2c_s^{-2} f_i^* \mathbf{c}_i\cdot\mathbf{u}_B & q\le\frac{1}{2} \\ \frac{1}{2q}\hat{f}_i^c(n,\mathbf{k}) + (1-\frac{1}{2q})\hat{f}_{i^*}^c(n,\mathbf{k}) + \\ \qquad \frac{1}{q}c_s^{-2} f_i^* \mathbf{c}_i\cdot\mathbf{u}_B & q>\frac{1}{2} \end{cases} \tag{13}$$

where $i^*$ is such that $\mathbf{c}_{i^*}=-\mathbf{c}_i$, $q\in[0,1)$ is the node-boundary distance along the link $\mathbf{c}_i$ and $\mathbf{u}_B$ is evaluated at

$$\mathbf{b}_i(\mathbf{k}) = \mathbf{x_k} + qh\mathbf{c}_i. \tag{14}$$

Notice that the variable $q$ can assume the value zero, since the interface $\Gamma$ has been considered as part of the computational fluid domain.

**Moving boundaries.** When the solid disk is moving through the computational domain according to the prescribed velocity, certain nodes which have

been solid nodes at time step $n$ will become fluid nodes in step $n+1$. Conversely, fluid nodes may disappear and become solid nodes. To deal with this problem, we use the method presented in [8] which amounts to an extrapolation of the missing information. This is needed for the practical implementation of the presented benchmarks. However, in the present context details concerning the movement are not relevant. In fact, the boundary forces are related to the state of the system (i.e. $p$ and $\nabla \mathbf{u}$) which is stationary (in leading order) for the test cases considered here. The special choice of the stationary solution is an expedient to have numerical results which do not depend on the particular algorithm chosen to deal with moving boundaries, since we do not consider this topic here. However, the following analysis is valid in general, also for time depending solutions.

**Momentum Exchange algorithm** Finally, we approximate the integral (2) using the *Momentum Exchange Algorithm* (MEA), proposed in its original form by Ladd[1], which allows to evaluate the interaction between fluid and boundary using directly the variables of LBM. The idea is to consider the momentum transferred to the solid from each *boundary fluid node* $\mathbf{x_k}$, interacting with the boundary along a link $\mathbf{c}_i$ (see fig. 1), given by the difference between the distributions moving in opposite directions

$$\phi_i(n,\mathbf{k}) = \mathbf{c}_i \hat{f}_i^c(n,\mathbf{k}) - \mathbf{c}_{i^*} \hat{f}_{i^*}(n+1,\mathbf{k}) = \mathbf{c}_i \left( \hat{f}_{i^*}(n+1,\mathbf{k}) + \hat{f}_i^c(n,\mathbf{k}) \right). \quad (15)$$

Defining the *boundary set*

$$B(\Gamma) = \left\{ (\mathbf{k},i) \in \mathbb{Z}^2 \times \mathbb{V} \mid \mathbf{x_k} \in \Omega_F \cup \Gamma, \mathbf{x_{k+c}}_i \in \Omega_S \right\} \quad (16)$$

which collects the boundary nodes and the directions crossing the boundary, the approximation of the force (denoted with $\hat{\mathbf{F}}$) acting on the boundary is obtained by taking the sum of all the contributions (15)

$$\hat{\mathbf{F}} = \sum_{(\mathbf{k},i)\in B(\Gamma)} \phi_i(n,\mathbf{k}). \quad (17)$$

In practice, the algorithm can be summarized as follows

**Algorithm 1**
*Construct the boundary set* $B(\Gamma)$ *(equation* (16)*)*
*Initialize* $\hat{\mathbf{F}} = 0$
`DO over` $B(\Gamma)$
  `LB-collision:` $\rightarrow \hat{f}_i^c(n,\mathbf{k})$
  `boundary condition:` $\rightarrow \hat{f}_{i^*}(n+1,\mathbf{k})$
  `momentum exchanged:` $\phi_i(n,\mathbf{k}) = \mathbf{c}_i \left( \hat{f}_{i^*}(n+1,\mathbf{k}) + \hat{f}_i^c(n,\mathbf{k}) \right)$
  `update:` $\hat{\mathbf{F}} = \hat{\mathbf{F}} + \phi_i(n,\mathbf{k})$
`end`

## 4 Numerical tests and asymptotic analysis

Algorithm 1 is now tested on the problem $CiF_0$. In absence of pressure, we compare the results for the local stresses, by evaluating the momentum exchanged *point by point* along the boundary, when the flow and the cylinder are fixed ($\mathbf{u}_0 = 0$), or both moving with the same velocity $\mathbf{u}_0 = (5, 0)$ (fig. 2). Despite the trivial exact solution $f_\mathbf{t} = f_\mathbf{n} = 0$, we observe the presence of local forces in relevant orders, *different* in the two cases and *highly irregular*, even if the pressure and the velocity over all the domain are exact.

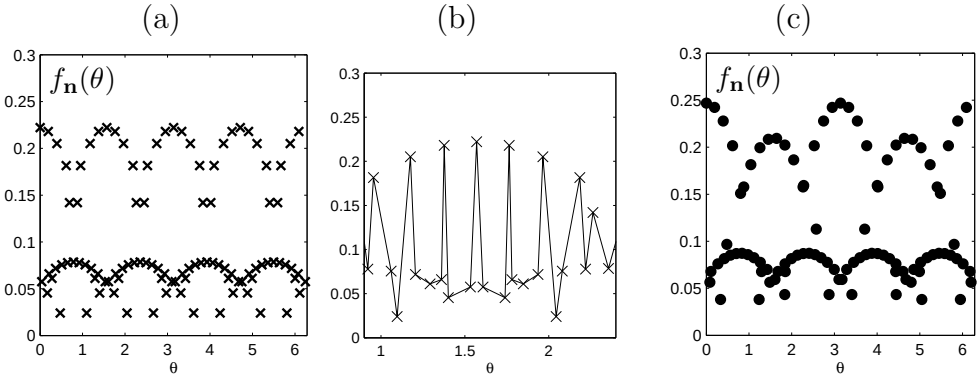


Figure 2. Results of the MEA for the normal stress $f_\mathbf{n}$, simulating $CiF_0$ on a $25 \times 25$ grid. For each boundary point $\mathbf{b}_i(\mathbf{k})$ the value computed with (15) at the corresponding node $\mathbf{x}_\mathbf{k}$ is drawn. The exact solution is $f_\mathbf{n} = 0$. **(a)** Flow at rest, $\mathbf{u}_0 = (0, 0)$. The results show strong oscillations. Note that consecutive points ($\times$) are not connected by lines for clarity. **(b)** Zoom on a small part of the boundary around the north pole $\theta = \frac{\pi}{2}$ now with connecting lines to demonstrate the oscillation. **(c)** Same model as in (a), but with $\mathbf{u}_0 = (5, 0)$. Galilean invariance is not satisfied (in the relevant order).

In order to understand this behavior, we investigate the properties of the algorithm assuming the LB solution to be representable as a sum [5]

$$\hat{f}_i(n, \mathbf{j}) = f_i^{(0)}(nh^2, \mathbf{j}h) + hf_i^{(1)}(nh^2, \mathbf{j}h) + h^2 f_i^{(2)}(nh^2, \mathbf{j}h) + \dots \,, \tag{18}$$

with coefficients $f_i^{(k)}$ sufficiently smooth and $h$-independent. Explicitly, the lower orders $f_i^{(k)}$ are derived by inserting equation (18) into (9) and into the boundary algorithm (13), Taylor expanding and sorting the orders in $h$. We have [5,7]

$$\begin{aligned} f_i^{(0)} &= f_i^*, \\ f_i^{(1)} &= f_i^* c_s^{-2} \mathbf{c}_i \cdot \mathbf{u}, \\ f_i^{(2)} &= f_i^* c_s^{-2} p + f_i^* \tfrac{c_s^{-4}}{2} \left( |\mathbf{c}_i \cdot \mathbf{u}|^2 - c_s^2 \mathbf{u}^2 \right) - \tau f_i^* c_s^{-2} (\mathbf{c}_i \cdot \nabla) \mathbf{c}_i \cdot \mathbf{u}, \end{aligned} \tag{19}$$

where $\mathbf{u}$ and $p$ solve the Navier-Stokes equations (1). In other words, the

*truncated expansion*

$$\hat{F}_i = f_i^{(0)} + h f_i^{(1)} + h^2 f_i^{(2)}, \tag{20}$$

predicts the LB solution up to order $h^3$. Since suitable velocity moments of $\hat{F}_i$ yield the Navier-Stokes solution $\mathbf{u}$, $p$ as well as the stress tensor $\mathbf{S}$, we conclude that the corresponding moments of $\hat{f}_i$ give rise to approximations of these fields. In particular,

$$\hat{\mathbf{u}} = \frac{\sum_i \mathbf{c}_i \hat{f}_i}{h}, \quad \hat{p} = c_s^2 \frac{\sum_i \hat{f}_i - 1}{h^2}. \tag{21}$$

are approximations of second order in $h$ for $\mathbf{u}$ and first order for $p$. The tensor $\mathbf{S}$ can be approximated (first order) by

$$\hat{\mathbf{S}}[\mathbf{u}] = -\frac{\nu}{\tau c_s^2 h^2} \sum_i \mathbf{c}_i \otimes \mathbf{c}_i \left( \hat{f}_i - f_i^{eq}(\hat{f}) \right). \tag{22}$$

To understand the behavior of the MEA, and to establish a connection between the values $\phi_i$ and the integral we want to compute, the results of the asymptotic analysis (summarized in (19)) are applied. For each couple $(\mathbf{k}, i) \in B$, the point $\mathbf{b}_i(\mathbf{k})$ defined in (14) is the intersection between $\Gamma$ and the link $\mathbf{c}_i$ from node $\mathbf{k}$. Inserting (19) into (15), taking into account equation (13) for the population $\hat{f}_{i^*}$, which are updated with the boundary algorithm, we obtain (dropping the time dependence for brevity)

$$\phi_i(\mathbf{k}) = \phi_i^{(0)}(\mathbf{x}_\mathbf{k}) + h^2 \phi_i^{(2)}(\mathbf{x}_\mathbf{k}) + O(h^3), \tag{23}$$

with

$$\begin{aligned} \phi_i^{(0)}(\mathbf{x}_\mathbf{k}) &= 2 f_i^* \mathbf{c}_i \\ \phi_i^{(2)}(\mathbf{x}_\mathbf{k}) &= 2 f_i^* c_s^{-2} \left( p + \frac{c_s^{-2}}{2} \left( |\mathbf{c}_i \cdot \mathbf{u}_B|^2 - c_s^2 \mathbf{u}_B^2 \right) - c_s^{-2} \nu \mathbf{c}_i \cdot \nabla \mathbf{u}_B \cdot \mathbf{c}_i \right) \mathbf{c}_i. \end{aligned} \tag{24}$$

All the quantities on the right hand sides of equations (23)-(24) are evaluated at the boundary point $\mathbf{b}_i(\mathbf{k})$. To better understand equation (24), we look at a simple example, with an horizontal boundary, on the top of the fluid flow (figure 3a).

In our notation for the discrete velocities (8), the last row of fluid nodes interacts with the solid along the directions $i = 2, 3, 4$. Computing explicitly the sum $\Phi(\mathbf{k}) = \phi_2(\mathbf{k}) + \phi_3(\mathbf{k}) + \phi_4(\mathbf{k})$ with equation (24), for a particular

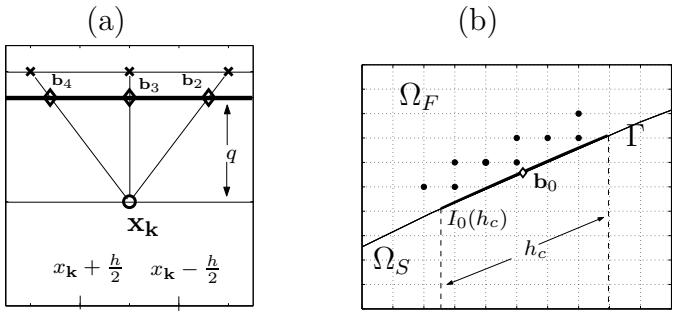


Figure 3. **(a)** Formula (24) for horizontal boundary. The points on the boundary ($\diamond$) where the functions are evaluated can be interpreted as nodes of a quadrature rule for the integral (2) over an interval of length $h$. The location of such nodes depends on the distance $q$. **(b)** Meaning of the *coarser grid* $h_c$ introduced in lemma 4.1. For a point $\mathbf{b}_0 \in \Gamma$ ($\diamond$), the local boundary $I_0(h_c)$ (bold line) can be identified as a ball centered in $\mathbf{b}_0$ and diameter $h_c$, intersected with the interface.The momentum exchange is evaluated at the points interacting with $I_0(h_c)$ (•).

boundary node $\mathbf{x_k}$, we have (omitting the dependence on $\mathbf{x_k}$ on the RHS)

$$\begin{aligned}\Phi(\mathbf{k}) = -\tfrac{1}{3}\begin{pmatrix}0\\1\end{pmatrix} + h^2\begin{pmatrix}-\frac{1}{2}[\mathbf{S}_{xy}(\mathbf{b}_2)+\mathbf{S}_{xy}(\mathbf{b}_4)]\\ \frac{1}{6}[p(\mathbf{b}_2)+4p(\mathbf{b}_3)+p(\mathbf{b}_4)]-\mathbf{S}_{yy}(\mathbf{b}_3)\end{pmatrix} + \\ +h^2\begin{pmatrix}\frac{1}{2}[u_B(\mathbf{b}_2)v_B(\mathbf{b}_2)+u_B(\mathbf{b}_4)v_B(\mathbf{b}_4)]\\ \frac{1}{6}[v_B(\mathbf{b}_2)+4v_B(\mathbf{b}_3)^2+v_B(\mathbf{b}_4)^2]\end{pmatrix} + O(h^3)\end{aligned} \tag{25}$$

The zero order term is responsible for the surplus of pressure, and is not related to integral (2). The second order is a combination of quadrature formulas over a small interval on the boundary for the functions $p$, $\mathbf{S}$, plus a quadratic function of velocity, which breaks the *Galilean invariance* (as happened in the test problem $\mathrm{CiF}^0$, fig.2).

After discovering the unwanted terms in expression (24), we can easily define a *corrected* momentum exchange algorithm, based on the values

$$\overline{\phi}_i(\mathbf{k}) = \phi_i(\mathbf{k}) - 2f_i^*\mathbf{c}_i - h^2 f_i^* c_s^{-4}\left(|\mathbf{c}_i\cdot\mathbf{u}_B(\mathbf{b}_i(\mathbf{k}))|^2 - c_s^2\mathbf{u}_B(\mathbf{b}_i(\mathbf{k}))^2\right)\mathbf{c}_i. \tag{26}$$

Using this modification, the simple test problem $\mathrm{CiF}_0$ with zero boundary stresses is now solved correctly.

We continue our analysis with problem $\mathrm{CiF}_1$ where a prescribed pressure distribution appears on the boundary. Results obtained with the modified MEA are shown in figure 4. Obviously, the approximation of the local stresses is still unsatisfactory. The numerical tests (fig.4) show a highly irregular behavior. Observe that the leading order of the expansion of the corrected momentum

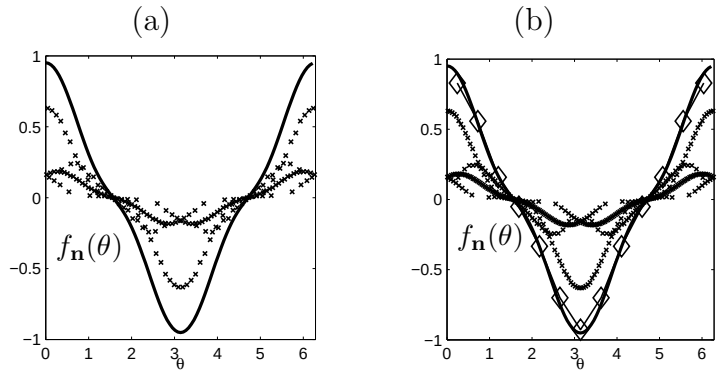


Figure 4. Problem $\mathsf{CiF}_1$ (pressure different from 0). **(a)** The symbols ($\times$) denote the values (26) for each boundary couple $(\mathbf{k}, i)$ versus the related point $\mathbf{b}_i(\mathbf{k}) \in \Gamma$, identified by $\theta \in [0, 2\pi)$, for a $50 \times 50$ grid. The solid line is the exact solution (6). The high frequence oscillation is explained by the $i$-dependence of the momentum exchange. In fact, along the interface two successive intersection points are in general related to different links $\mathbf{c}_i$. **(b)** Results using a $100 \times 100$ grid. The approximation on the fine scale is more noisy, but does not improve (compare with (a)) the approximation of the local stresses. The values, sampled by the crosses $\times$ are strongly oscillating, on a very dense grid, which seems to result in different solid lines (similar to what appeared in figure 2c). Averaged values, computed grouping the points according to a grid $h_c = h^{0.5}$ ($\diamond$), are indicated by diamonds.

exchange (26) consists now only of the corrected second order coefficient

$$\phi_i^{(2)}(\mathbf{x_k}) = 2 f_i^* c_s^{-2} \left( p(\mathbf{b}_i(\mathbf{k})) - c_s^{-2} \nu \mathbf{c}_i \cdot \nabla \mathbf{u}_B(\mathbf{b}_i(\mathbf{k})) \cdot \mathbf{c}_i \right) \mathbf{c}_i. \qquad (27)$$

It contains the pressure and the gradient of velocity evaluated at the boundary point $\mathbf{b}_i(\mathbf{k}) \in \Gamma$. However, the weights multiplying the functions in equation (27) depend on the direction $\mathbf{c}_i$. In the special case of horizontal boundary the sum of momentum exchange in a boundary node (25) had a clear relation with an approximate integration rule. Since for general curved boundary the distribution of these points and the outgoing directions along the interface is in general irregular, the momentum exchange in a single boundary node might not be directly related to an approximation of the stresses on the interface.

### *4.1 Averaging the momentum exchange*

Moreover, using directly the momentum exchange $\overline{\phi}_i(\mathbf{k})$ as approximation of the stress in the point $\mathbf{b}_i(\mathbf{k})$ allows only to define the boundary interaction in special points (the intersections between grid and lattice). In other words, the MEA does not allow to define the force acting on an arbitrary $\mathbf{b} \in \Gamma$. To overcome this problem, we have analyzed an *averaged* value of the momentum exchanged along small intervals on the boundary.

In practice, we choose a point $\mathbf{b}_0 \in \Gamma$ and a coarse grid size $h_c > h$. The approximation of the local force in $\mathbf{b}_0$ is computed summing all the momentum exchange contributions (with a proper weight relating $h$ and $h_c$) of the couples $(\mathbf{k}, i) \in B(\Gamma)$ such that the corresponding $\mathbf{b}_i(\mathbf{k})$ belongs to an $h_c$ neighborhood of $\mathbf{b}_0$. This leads to better results (fig. 4b).

Formalizing the procedure, we have the following result (valid also for the three dimensional $D3Q15$ model):

**Lemma 4.1** *Let $\mathbf{b}_0 \in \Gamma$ be a point on a smooth d-dimensional interface ($d = 1, 2$). Given the LB-grid size $h$, we consider a* coarser *grid $h_c$, such that $h = o(h_c)$. The related interval is given by $I_0(h_c, \mathbf{b}_0) = \left\{ \mathbf{b} \in \Gamma : |\mathbf{b} - \mathbf{b}_0| < \dfrac{h_c}{2} \right\}$. Defining local averages of the exact and approximate normal stress in $I_0$*

$$\mathcal{I}(\mathbf{b}_0, h_c) = \frac{1}{h_c^d} \int_{I_0} (-p\mathbf{I} + \mathbf{S}) \cdot \mathbf{n} \, d\sigma,$$

$$\hat{\Phi}(\mathbf{b}_0, h_c) = \left( \frac{h}{h_c} \right)^d \sum_{(\mathbf{k},i):\mathbf{b}_i(\mathbf{k}) \in I_0} \frac{\overline{\phi}_i(\mathbf{k})}{h^2}$$

*the following estimate holds*

$$\left| \mathcal{I}(\mathbf{b}_0, h_c) - \hat{\Phi}(\mathbf{b}_0, h_c) \right| = O\left( h_c + \frac{h}{h_c} \right). \tag{28}$$

The proof is based on writing the sum $\hat{\Phi}(\mathbf{b}_0, h_c)$ in terms of the functions $p$ and $\mathbf{S}$ using equation (24) combined with a Taylor expansion around the node $\mathbf{b}_0$. The resulting expressions can be viewed as approximate integration rules on the interface. Unfortunately, the weights of the arising quadrature formulas do not sum up exactly to one at every node which rules out first order accuracy. However, using some arithmetical properties of the weights, it can be shown that the deviation from one goes to zero if the weights are summed over subsets of the interface which are large compared to the grid size $h$ of the regular grid. On the other hand, the Taylor approximation is less accurate if it is used on a coarse mesh of typical distance $h_c$. Hence, a balance between fine and coarse grid arises in equation (28), and to obtain an optimal error bound, a good compromise is required.

**Optimal coarsening.** *Choosing $h_c = \sqrt{h}$, equation (28) gives*

$$\left| \mathcal{I}(\mathbf{b}_0, \sqrt{h}) - \hat{\Phi}\left(\mathbf{b}_0, \sqrt{h}\right) \right| = O\left(\sqrt{h}\right). \tag{29}$$

To validate the result of lemma 4.1, we compare the momentum exchange evaluated along the boundary point in problem $CiF_1$, averaged according to

several coarser grids of type $h_c = h^\alpha$. The order plot in fig. 5 confirms that the best rate of error decay is obtained choosing $h_c = \sqrt{h}$.

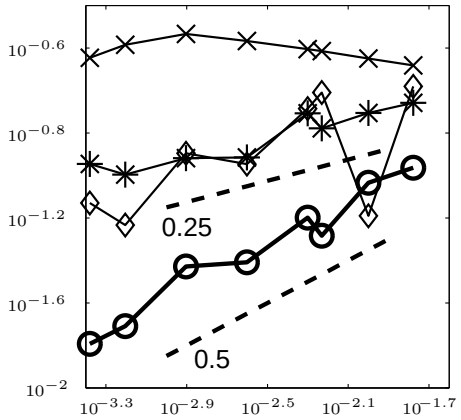


Figure 5. Double logarithmic plot of the error in the local forces versus the grid size $h$. Comparisons of different coarser grids $h_c = h^\alpha$, with $\alpha = 0.25(\diamond), 0.5(\circ, \text{bold line}), 0.75(*), 0.9(\times)$. The dashed lines represent reference slopes.

## References


[1] A.J.C. Ladd. Numerical simulations of particular suspensions via a discretized Boltzmann equation. Part 2 (Numerical results) *J. Fluid Mech.*, **271**:311–339, 1994.

[2] R.Mei, D.Yu, W.Shyy, L.-S. Luo. Force evaluation in the lattice Boltzmann method involving curved geometry. *Phys. Rev. E*, **65**:041203, 2002.

[3] H.Li, X.Lu, H.Fang, Y.Qian. Force evaluations in lattice Boltzmann simulations with moving boundaries in two dimension. *Phys. Rev. E*, **70**:026701, 2004

[4] S.Succi. *The Lattice Boltzmann Equation for Fluid Dynamics and Beyond.* Oxford University Press, 2001.

[5] M.Junk, A.Klar, L.-S.Luo. Theory of the Lattice-Boltzmann method: Mathematical Analysis of the Lattice Boltzmann equation. To appear on *J. Comp. Phys.*, 2005.

[6] M.Bouzidi, M.Firdaouss, P.Lallemand. Momentum transfer on a Boltzmann lattice fluid with boundaries. *Physics of Fluids*, **13**:4823–4842, 1993.

[7] M.Junk, Z.Yang. Asymptotic Analysis of lattice Boltzmann Boundary Conditions. To appear on *J. Stat. Phys.*, 2005

[8] P.Lallemand, L.-S. Luo. Lattice Boltzmann method for moving boundaries. *J. Comp. Phys.*, **184**:3452-3458, 2001.